IEEE Access
Multidisciplinary | Rapid Review | Open Access Journal

Received April 21, 2020, accepted May 1, 2020, date of publication May 6, 2020, date of current version May 19, 2020.

Digital Object Identifier 10.1109/ACCESS.2020.2992836

Improved Generative Adversarial Network-Based Super Resolution Reconstruction for Low-Frequency Measurement of Smart Grid

FUSHENG LI, DAN LIN, AND TAO YU, (Member, IEEE)
School of Electric Power, South China University of Technology, Guangzhou 510640, China
Guangdong Key Laboratory of Clean Energy Technology, South China University of Technology, Guangzhou 510641, China

Corresponding author: Tao Yu (taoyu1@scut.edu.cn)

This work was supported in part by the National Natural Science Foundation of China under Grant 51777078, in part by the Key Projects of Basic Research and Applied Basic Research in Universities of Guangdong Province under Grant 2018KZDXM001, and in part by the Funding of Key Projects of Basic Scientific Research Operating Expenses of Central Universities.

ABSTRACT There is a universal trend toward a data-driven smart grid, which aims to realize two-way communication of energy flow and data flow between various agents across power generation side, transmission& distribution side, electricity retailors and end users. However, the low frequency electrical measurement data accumulated over a long period of time is insignificant for intelligent agents. This paper presents a machine learning method for reconstructing the low frequency electrical measurement data in smart grid. Firstly, the electrical measurement data is converted into electrical images, and then the low frequency electrical measurement data is reconstructed into high frequency electrical measurement data by generative adversarial network to improve the training stability, Wasserstein distance is introduced into the reconstruction mechanism. In addition, by designing the deep residual network based generator, the deep convolutional network based discriminator as well as the perception loss function, the reconstruction accuracy and the high-frequency detail reduction ability are improved. The proposed method is tested on three publicly available datasets and compared with the traditional data reconstruction method, justifying that this method not only can restore high-frequency details with less error, but also can be generalized to different datasets at one location and to datasets at different locations with satisfactory accuracy.

INDEX TERMS Data-driven, super-resolution reconstruction, generative adversarial network, electrical measurement data.

I. INTRODUCTION

Smart grid is considered as the next generation power grid, which builds a widely distributed automated energy transmission network facilitating the data exchange and energy transmission among various agents of power generation, transmission, distribution, electricity sale and electricity consumption [1]. The intelligence degree of contemporary artificial intelligence is closely related to the utilization degree of data. Intelligent technology characterized by deep utilization of data will be the core field of future electric power development. Smart grid places higher requirements on technologies such as data communication [2], data-driven [3], multi-energy management [4], [5], multi-agent optimization and control [6].

High quality data is the premise a data-driven smart grid. There are two kinds of data communications, including transmitting data from the sending end to the data center, and from the data center back to the receiving end [7]. However, a large amount of low-frequency electrical measurement data is collected in the current power system for three main reasons. First, the data sender can only install smart meters with low sampling frequencies due to insufficient economic capacity or technical constraints. The second is that although smart meters can be installed at the data sending end with high sampling frequency, the high-frequency electrical measurement data has to be compressed before transmission due to the traffic restrictions of communication equipment. Third, high-frequency electrical measurement data puts a lot

The associate editor coordinating the review of this manuscript and approving it for publication was Jiayong Li.

of storage pressure on the data center. Consequently, the low-frequency electrical measurement data received by the data receiver is only the average or maximum value of each sampling period [8], resulting in a lack of high-frequency detail information.

Until the above problems are solved economically and technically, the research on the compression mechanism and reconstruction mechanism has important significance for the advancement of the smart grid. At present, some pioneering research on the compression mechanism has been carried out, e.g., an automatic encoder to extract the corresponding structure from the electrical measurement data [7]. However, there are few studies on the reconstruction mechanism. Reference [9] used active power and voltage phase angle as state variables for data compression and linear interpolation for data reconstruction. However, the reconstruction accuracy obtained by the interpolation method is unsatisfactory. Reference [10] realized the reconstruction of missing data in power system state estimation through shallow auto-encoder neural networks, but it is difficult for shallow networks to accurately describe the complex spatiotemporal characteristics of electrical measurement data. References [11]–[13] implemented high-precision reconstruction of missing data through generative adversarial networks, matrix filling, and graph regularized low-rank matrix recovery methods, respectively, but did not involve the improvement of the electrical measurement data sampling frequency.

The essence of image super-resolution reconstruction is similar to that of electrical measurement data. Both are difficult to model and restore high-frequency details. There are three main types of super-resolution reconstruction methods in the image field, including interpolation-based methods, modeling-based methods, and learning-based methods. Among them, the interpolation-based methods such as adaptive interpolation algorithms [14] are visually too smooth and inevitably lose edge detail information, while typical methods such as Bayesian analysis [15], maximum posterior probability estimation [16] require a huge size of the solution space and is likely to result in excessive calculation and multiple solutions, based on its basic principle to reconstruct a high-resolution image solution space from a large number of low-resolution images. By contrast, the learning-based method solves the shortcomings of interpolation-based or modeling-based methods. For example, [17] applies sparse coding algorithms to super-resolution image reconstruction, but it tends to be smooth processing visually, and the restoration degree of high-frequency details is insufficient.

In recent years, generative adversarial network (GAN) [18] not only has made breakthrough progress in the fields of images and texts [19], [20], but also is widely applied in the electrical field [21], [22]. With the help of a trained discriminator network, GAN distinguishes super-resolution images from real images, in order to solve natural image manifolds and learn complex spatio-temporal relationships unsupervised from historical data. Reference [23] has introduced Wasserstein distance in the training target, which improves the stability of the GAN training process. Reference [24] has designed a GAN structure for image super-resolution reconstruction and introduced perceptual loss, which improved the ability of GAN to restore high-frequency details.

In this paper, a generative adversarial network based super-resolution reconstruction method for low-frequency electrical measurement data in smart grid is proposed. The contributions of work are listed as follows:

1) A method for transforming electrical measurement data into electrical images is designed so that the GAN can effectively learn the potential distribution of electrical measurement data with the help of image processing techniques.

2) The Wasserstein distance is introduced into the GAN model to avoid the disappearance of the gradient of the GAN, which improves the training stability.

3) Three designs are involved, including a generator based on deep residual network, a discriminator based on deep convolutional network, and a perceptual loss function, so that the reconstruction accuracy of GAN can be improved.

4) The proposed method is a data-driven based unsupervised training method. The generalization of the proposed method in different data sets at the same geographical location and its applicability in different data sets at different geographical locations are verified.

The rest of the paper is organized in the following sequence. Section II develops the data flow in smart grid. Section III proposes a super-resolution reconstruction method of low-frequency electrical measurement data based on improved GAN. Section IV simulation experiment verifies the feasibility of the proposed method. Section V concludes the paper.

II. DATA FLOW IN SMART GRID

Nowadays, a large number of smart meters have been configured to collect data which has the following characteristics: On the one hand, the acquisition frequency is low. At present, the sampling frequency of most publicly available power datasets is at the levels of 15min, 30min, and 1h, but only a few reaches the level of 1min or 1Hz. On the other hand, there are few datasets with high collection frequency and large coverage. As shown in Table 1, it is difficult for the existing publicly available electrical measurement datasets to simultaneously guarantee high acquisition frequency and large

TABLE 1. Details of publicly available electrical measurement datasets.

Dataset	Location	Houses	Datatype	Sampling rate
DRED[25]	NED	1	P	1Hz
IHEPCds[26]	FRA	1	P,Q,V,I	1min
AMPds2[27]	CAN	1	P,Q,S,V,I,f,pf	1min
I-BLEND[28]	IND	7	P,V,I,f,pf	1min
HES[29]	UK	251	P	10min

Acronyms: NED→Netherlands, FRA→France, CAN→Canada, IND→India, UK→United Kingdom, P→Active power, Q→Reactive power, S→Apparent power, V→Voltage, I→Current, f→Frequency, pf→Power frequency.

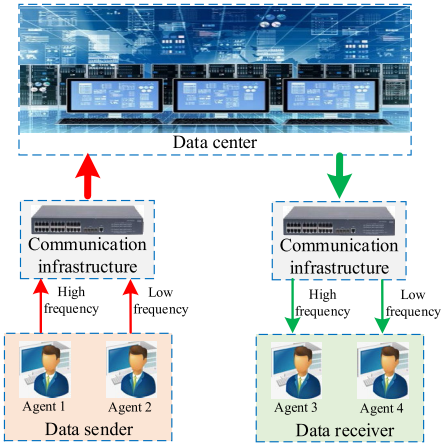

FIGURE 1. Data flow pattern of traditional grids.

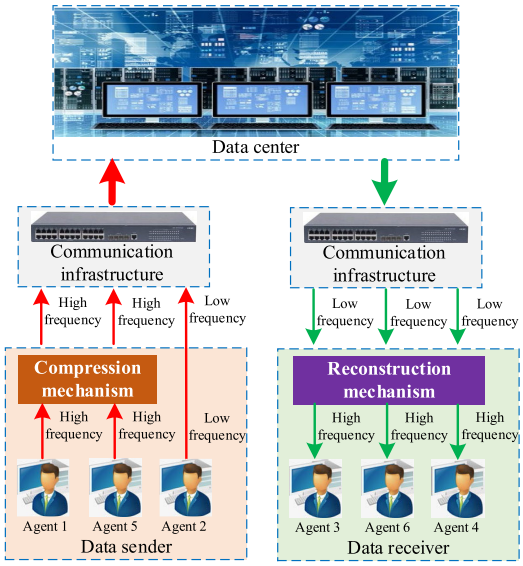

FIGURE 2. Data flow pattern of smart grids.

coverage. High acquisition frequency means high equipment investment, communication, and high cost of data storage. Therefore, high frequency datasets generally involve only a small number of users and a small amount of measurement data types. Similarly, large-coverage datasets are generally low-frequency datasets due to the requirement: to install a large number of equipment and collect many data types.

In addition to economic and technical constraints, the compression mechanism of the smart grid is also an important factor resulting in a large amount of low-frequency electrical measurement data. The smart grid operates through the agents in the five kinds of data flows between power generation, transmission, distribution, electricity market, and power consumption. As shown in Figure 1, the data flow mode of the traditional power grid is to first transmit the data collected by the data sender from the installed electricity meter through the communication infrastructure and store it in the data center. Then the data is transmitted through the communication infrastructure and directly utilized at the data receiver. Obviously, this model has two major disadvantages. One is that the communication and storage of high-frequency data brings a heavy burden on the economy and technology while the other is that the value of low-frequency data cannot be fully tapped.

To promote the development of smart grids, typical advanced data flow mode becomes to collect data from the installed smart meters, and use a compression mechanism to compress high-frequency data in place, as shown in Figure 2. Low-frequency data is transmitted through the communication infrastructure and stored in the data center, and then transmitted through the communication infrastructure and reconstructed into high-frequency data through the reconstruction mechanism at the data receiver. Obviously, this model has two major advantages. One is that benefitting from in-place compression and in-place reconstruction, data processing changed from a centralized manner to a distributed one, which has greatly reduced the computing pressure of the data center. The second is that only low-frequency data is the communication infrastructure transmits, so that more datasets can be transmitted under the same bandwidth, which improves communication efficiency.

It must be pointed out here that this paper discusses the reconstruction of low frequency measurement data in smart grid, not other processes of data flow. In the following content, this paper proposes an algorithm based on machine learning to reconstruct low-frequency electrical measurement data for smart grid.

III. SUPER-RESOLUTION RECONSTRUCTION METHOD OF LOW-FREQUENCY ELECTRICAL MEASUREMENT DATA BASED ON IMPROVED GAN

Super resolution reconstruction, which involves data transformation from a low-dimensional space to a high-dimensional one, is a highly ill-conditioned inverse problem which has a large number of feasible solutions [24]. Based on the most advanced progress in super-resolution image reconstruction, this paper proposes to convert electrical measurement data into so-called electrical images, where data for different kinds of electrical measurements are saved in different color channels while the pixel elements in one channel represents measured data at a sampling time moment. Compared with the traditional single-layer and one-dimension data flow, elegant merits of electrical image are that multiple kinds of measurement data can be transmitted by using multiple channels while larger amount of data can be stored with nearly the same storage by realigning the original data vector into a two-dimensional data matrix. Clearly, the higher frequency the samples are, the higher resolution the corresponding electrical image channel will be and the more storage resources are required. As mentioned before, low-resolution images are preferable to be transmitted for economical concern and are to

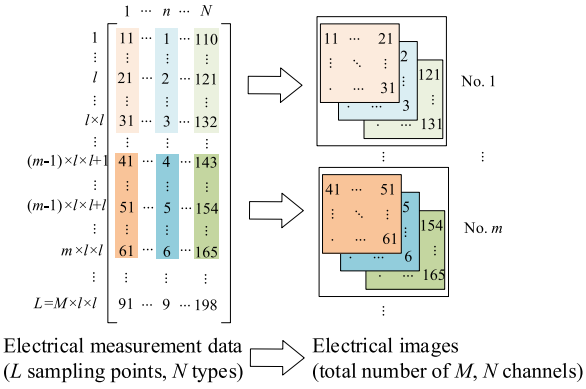

FIGURE 3. Method adopted for converting electrical measurement datasets into electrical images.

TABLE 2. The entire execution of transforming electrical measurement data into electrical images.

1: Extract the n-th type of high-frequency electrical measurement data, where $1 \le n \le N$.
2: **FOR** $n := 1$ to N
3: Re-assemble data vector of size l ^ 2 ×1 in to a $l \times l$ matirx where l is a positive and a composite integer. Specifically, data in the l - 1 column in the matrix is earlier than that in the lth column. A total of M low-dimension matrices (i.e., electrical images) are formed in case of overfitting.
4: **END FOR**
5: **FOR** $m := 1$ to M
6: **FOR** $n := 1$ to N
7: The m-th 2-dimensional matrix after recombining the n-th type of high-frequency electrical measurement data is stored in the m-th channel of the n-th image of the high-resolution electrical image.
8: **END FOR**
9: **END FOR**
10: Store the high-resolution electrical images of M 2-dimensional N-channel obtained in the foregoing steps.

be reconstructed back into a high-resolution one by the super-resolution reconstruction technique.

A. TRANSFORM ELECTRICAL MEASUREMENT DATA INTO ELECTRICAL IMAGES

Assuming that the high-frequency electrical measurement data set includes N types of electrical measurement data, such as active power, reactive power, voltage, current, frequency, power factor, and so on. The original high-frequency electrical measurement dataset can be expressed as a matrix of $L \times N$, where L denotes the total number of samples at different time moments. Each channel is a two-dimensional matrix derived from the original data vectors, as shown in Figure 3. The steps are shown in Table 2.

B. MECHANISM OF SUPER RESOLUTION RECONSTRUCTION

The super-resolution reconstruction mechanism with GAN introduced is shown in Figure 4, which includes training stability enhancement, design of the generator and the discriminator structures, and the loss function development. The low-resolution electrical images are put into a trained

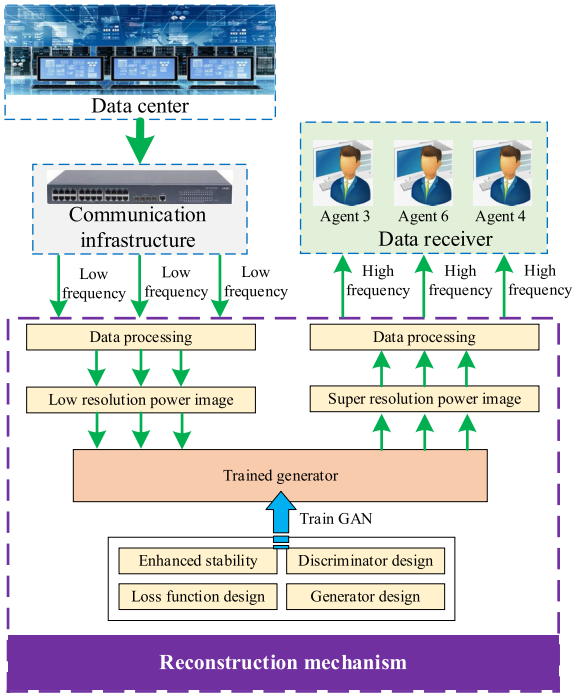

FIGURE 4. Super resolution reconstruction framework based on improved GAN.

generator by which a super-resolution electrical image is obtained. Finally, pixels in the super-resolution electrical images are converted back yielding high-frequency electrical measurements.

C. GENERATIVE ADVERSARIAL NETWORK

GAN is a new neural network architecture proposed by Goodfellow in 2014, which consists of a generator and a discriminator. The generator provides a sample that is similar to the real sample but indistinguishable, while the discriminator distinguishes the difference between the two samples [30].

The GAN-based super-resolution reconstruction method for low-frequency electrical measurement data generates super-resolution electrical images by training a generator. Then, the discriminator screens out a large number of possible solutions from the generated samples with the minimal difference from the actual situation, thereby solving the highly ill-conditioned inverse problem. In addition, unlike a learning-based method that uses only one neural network, GAN uses two neural networks as generators and discriminators, respectively, resulting in stronger data distribution learning capabilities. The reason is that the discriminator directly compares the difference in potential data distribution between the generated data and the real data, thus replacing the error calculation part of the generator.

The GAN structure of the proposed method is shown in Figure 5. The real high-resolution electrical image set, the real low-resolution electrical image set and the super-resolution electrical image set are x^{HR}, x^{LR}, and x^{SR},

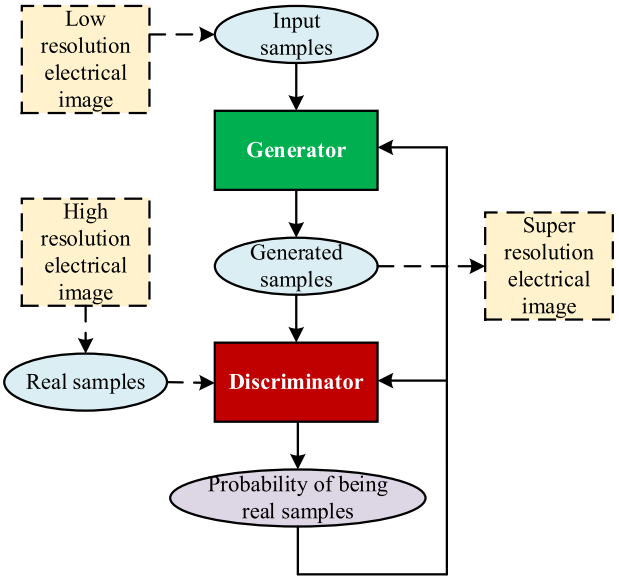

FIGURE 5. GAN structure for super resolution reconstruction.

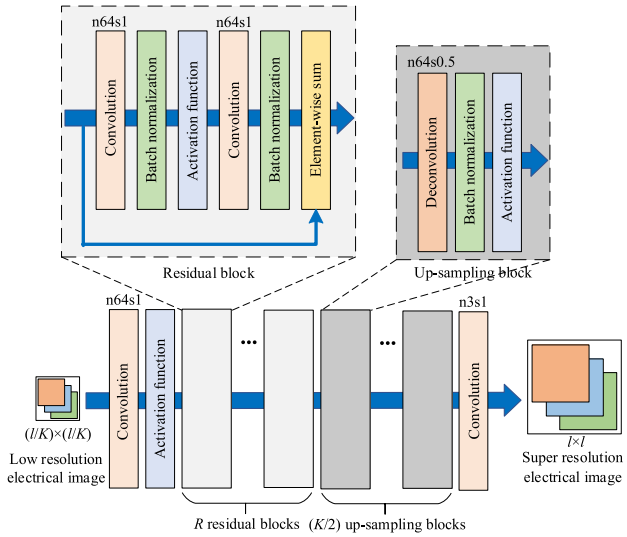

FIGURE 6. Generator structure for super resolution reconstruction.

respectively, whose probability distribution $p_{\mathrm{H}}(x^{\mathrm{HR}})$, $p_{\mathrm{L}}(x^{\mathrm{LR}})$, and $p_{\mathrm{S}}(x^{\mathrm{SR}})$ that are difficult to express explicitly through mathematical models. x^{SR} can also be expressed as $G_{\theta_{\mathrm{G}}}(x^{\mathrm{LR}})$, where θ_{G} is the parameter of the generator. Since the generator is able to counterfeit, discrimination cannot distinguish whether the input is real data or not so that it outputs a probability for generated sample i.e., $D_{\theta_{\mathrm{D}}}(G_{\theta_{\mathrm{G}}}(x^{\mathrm{LR}}))$ and real sample, i.e., $D_{\theta_{\mathrm{D}}}(x^{\mathrm{HR}})$, where θ_{D} is the parameter of the discriminator.

The training process of GAN is to optimize a min-max zero-sum game problem that its objective function is as follows.

$$\min_{\theta_{\mathrm{G}}}\max_{\theta_{\mathrm{D}}}\sum_{m}^{M}\log(D_{\theta_{\mathrm{D}}}(x_m^{\mathrm{HR}}))+\sum_{m}^{M}\log(1-D_{\theta_{\mathrm{D}}}(G_{\theta_{\mathrm{G}}}(x_m^{\mathrm{LR}}))) \tag{1}$$

The above formula reflects the adversarial game between the generator and the discriminator. The generator tries to reduce the difference between the generated sample and the real sample, while the discriminator recognizes the difference. When the discriminator can no longer recognize this difference, the game reaches an equilibrium.

D. ENHANCEMENTS TO THE STABILITY OF TRAINING

As mentioned above, although GAN can theoretically generate following complex spatiotemporal laws, it is likely to diverge in actual training. The reason is that GAN measures the distance between $p_{\mathrm{S}}(x^{\mathrm{SR}})$ and $p_{\mathrm{H}}(x^{\mathrm{HR}})$ as KL divergences or JS divergences. When the overlap of the two distributions is small to a certain extent or does not exist, the gradient disappears and the model collapses. To improve the stability of GAN training, this paper introduces the Wasserstein distance to modify formula (1). The objective function of GAN is shown as follows.

$$\min_{\theta_{\mathrm{G}}}\max_{\theta_{\mathrm{D}}}\sum_{m}^{M}D_{\theta_{\mathrm{D}}}(x_m^{\mathrm{HR}})-\sum_{m}^{M}D_{\theta_{\mathrm{D}}}(G_{\theta_{\mathrm{G}}}(x_m^{\mathrm{LR}})) \tag{2}$$

Compared with formula (1), formula (2) removes the logarithm operation, and each iteration of the actual training process needs to cut the discriminator parameters in a fixed range [-c, c], generally set c = 0.01.

E. GENERATOR

In this paper, deep residual network (DRN) is taken as the generator. Instead of only transmitting outputs to the next layer, output of DRN in a layer can span several layers, which alleviates the problem of gradient disappearance caused by increasing depth in a deep neural network. Besides, the superimposed multilayer residual blocks can improve the model's feature learning ability and accuracy [31].

The structure of the generator is shown in Figure 6. The low-resolution electrical image is considered as the input of the generator and is mapped into the hidden layer space through a convolution layer and an activation function layer. To speed up the training, the DRN is initialized with the pre-training results of VGG-19 [32]. DRN consists of R residual blocks, which have the same structure, including a convolution layer, a batch normalization layer, an activation function layer, a convolution layer, a batch normalization layer, and an element-wise sum layer. The magnification of each up-sampling block is two to improve the resolution of the reconstructed image. Obviously, when the reconstruction multiple is K, there are $(K/2)$ up-sampling blocks between the DRN and the output. Each up-sampling block includes 3 layers, namely a deconvolution layer, a batch normalization layer, and an activation function layer. In addition, some terms for convolution operations are also involved. n64s1 indicates that the convolution kernel of the convolution

layer has 64 channels and the sliding step of the convolution kernel is 1. n64s0.5 and n3s1 are similar to the expression of n64s1. All convolutional layers and deconvolutional layers use a 3 × 3 convolution kernel.

F. DISCRIMINATOR

Different from the generator, the discriminator mainly implements the classification of real samples and generated samples. Deep convolutional network (DCN), one of the core algorithms in the field of image recognition, has excellent performance in classification [33], which is used as the discriminator as shown in Figure 7.

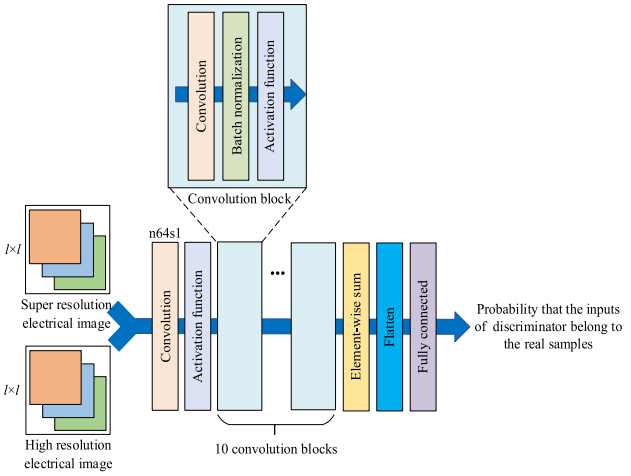

FIGURE 7. Discriminator structure for super resolution reconstruction.

The input is mapped into the hidden layer space through a convolutional layer and an activation function layer. The DCN consists of 10 convolutional blocks, each of which includes a convolutional layer, a batch normalization layer, and an activation function layer. The number of channels of the convolution kernel of the 10 convolution blocks is 128, 256, 512, 1024, 2048, 1024, 512, 128, 128, and 512. The convolution kernel size of the first 5 convolution blocks is 4 × 4 and the sliding step size is 2. The convolution kernel size of the 6th, 7th, and 8th convolution blocks is 3 × 3 and the sliding step size is 1. The convolution kernel size of the 9th and 10th convolution blocks is 1 × 1 and the sliding step size is 1. The deep convolutional network is followed by 1 element -wise sum layer, 1 flatten layer, and 1 fully connected layer. The above activation functions are all regarded as leaky ReLU, for the reason that it is able to improve the recognition accuracy of discriminator by avoiding pooling operation. In the end, discriminator outputs a probability value, which means the probability that the input of the discriminator belongs to a real sample.

G. LOSS FUNCTION

1) GENERATOR LOSS FUNCTION

In order to improve the reconstruction accuracy and high-frequency detail restoration ability, the generator loss function is designed as a weighted combination of the following loss functions.

Generative adversarial loss is generated according to the formula (2). By adding the result of discriminator to generative adversarial loss, the generator can deceive the discriminator. The calculation formula for Generative adversarial loss is as follows.

$$l_{\text{Gen}} = -\sum_{m=1}^{M} D_{\theta_{\text{D}}}(G_{\theta_{\text{G}}}(x_m^{\text{LR}})) \tag{3}$$

In this paper, the mean square error (MSE) of the generated sample and the real sample is taken as the actual loss. The formula for calculating actual loss is as follows.

$$l_{\text{MSE}} = \frac{1}{l^2}\sum_{m=1}^{M}\sum_{w=1}^{l}\sum_{h=1}^{l}((x_m^{\text{HR}})_{w,h} - (G_{\theta_{\text{G}}}(x_m^{\text{LR}}))_{w,h})^2 \tag{4}$$

where w and h are the width and height of the matrix in each channel, respectively.

The fact that the generator is trained with actual loss may result in smooth generated samples and conservative reconstruction results, which is not conducive to the restoration of high-frequency details. Thus, this paper introduces the perceptual loss to measure the difference in local features between the generated samples and the real samples. Specifically, considering that the VGG-19 model has the ability to extract local features of the electrical image, the generated samples and actual samples are input in the trained VGG-19 model, so that the feature map of the electrical image is extracted $\varphi_{a,b}$, where the meaning of $\varphi_{a,b}$ is the b-th feature map obtained by the VGG-19 model before the a-th pooling operation. The mean square error between each pixel point $\varphi_{a,b}(x^{\text{HR}})_{w,h}$ of feature maps corresponding to actual samples and each pixel point $\varphi_{a,b}(G_{\theta_{\text{G}}}(x^{\text{LR}}))_{w,h}$ of feature maps corresponding to generated samples is called the perceptual loss, which is calculated as

$$l_{\text{VGG}} = \frac{1}{l^2}\sum_{m=1}^{M}\sum_{w=1}^{l}\sum_{h=1}^{l}(\varphi_{a,b}(x_m^{\text{HR}})_{w,h} - \varphi_{a,b}(G_{\theta_{\text{G}}}(x_m^{\text{LR}}))_{w,h})^2 \tag{5}$$

In summary, the generator loss function is as follows.

$$l_{\text{G}} = \lambda_1 l_{\text{Gen}} + \lambda_2 l_{\text{MSE}} + \lambda_3 l_{\text{VGG}} \tag{6}$$

where $\lambda_1 = 1 \times 10^{-3}$, $\lambda_2 = 1$, and $\lambda_3 = 2 \times 10^{-6}$.

2) DISCRIMINATOR LOSS FUNCTION

Discriminated adversarial loss, obtained according to formula (2), is considered as the discriminator loss function.

The discriminator can discriminate the authenticity by adding results of discriminator to discriminated adversarial loss, which is calculated as follows.

$$l_{\text{D}} = \sum_{m=1}^{M} D_{\theta_{\text{D}}}(G_{\theta_{\text{G}}}(x_m^{\text{LR}})) - \sum_{m=1}^{M} D_{\theta_{\text{D}}}(x_m^{\text{HR}}) \tag{7}$$

IV. SIMULATION ANALYSIS

In order to test the reconstruction effect of the super-resolution reconstruction method proposed in this paper, three cases are carried out in this section:

- Case 1: use I-BLEND dataset to present a comparison between the performance of the super-resolution reconstruction method and the interpolation method.
- Case 2: use the datasets about different buildings in I-BLEND dataset to study the generalization of different datasets in the same geographical location.
- Case 3: uses the datasets I-BLEND, AMPds2, and IHEPCds from India, Canada, and France, respectively, to study the applicability of the super-resolution reconstruction method in different geographic datasets, and the generalization of the trained model in different geographic datasets.

The number of iterations in this study is set to be 5000. Moreover, Adam is used as the optimizer. The exponential decay rate of the first-order moment estimation of the optimizer is set to be while the initial learning rate of the optimizer is 1×10^{-4} which becomes $1/10$ of the initial after every 500 iterations.

A. DATA PREPARATION

1) FILLING UP MISSING VALUES

In this study, relatively complete data fragments are intercepted as experiment data, whose missing data amount is trivial and can be filled up by linear interpolation.

2) NORMALIZATION

In order to improve the visualization effect of the power image, the electrical measurement data is normalized to the commonly used value range of the image, which is [0, 255]

$$x_{mn} = \frac{x'_{mn} - \min(x'_{mn})}{\max(x'_{mn}) - \min(x'_{mn})} \times 255 \tag{8}$$

where x'_{mn} and x_{mn} represent the matrix before and after normalization of the n-th channel of the m-th electrical image, respectively. $\max(x'_{mn})$ and $\min(x'_{mn})$ are the maximum and minimum values of x'_{mn}, respectively.

3) DATASETS PARTITIONING

The three public data sets used in this study are shown in table 3, and 691,200 samples are taken for simulation. For the I-BLEND dataset, four buildings from the same school are selected, namely, Academic building, Boys dormitory, Girls dormitory, and Restaurant. The remaining two are data sets on the electricity consumption of one residential building.

It should be pointed out that the main purpose of this paper is to reconstruct the low-frequency data in Figure 2 into high-frequency data. Thus, in this paper, three high-frequency data sets are used for simulation, and the corresponding low-frequency data is used for reconstruction, in order to verify the reconstruction effect by comparing the differences between the reconstructed high-frequency data and the real high-frequency data.

TABLE 3. Experimental datasets.

Dataset	Period	Building	Datatype	Sampling rate
I-BLEND	2014-01-08 00:00-2015-05-02 23:59	4	P, I, V	1min
AMPds2	2012-04-01 15:00-2013-07-25 14:59	1	P, Q, I	1min
IHEPCds	2006-12-16 00:00-2008-04-08 23:59	1	P, Q, V	1min

The reconstruction multiple is K. In order to facilitate the construction of low-resolution electrical images, let K be a factor of the composite number l, then the total number of samples of low-frequency electrical measurement data is $(l/\sqrt{K})$, which means K high-frequency samples are taken in order of time. The maximum value of the electrical measurement data is taken as one sampling point of the low-frequency electrical measurement data. The steps for transforming low-frequency electrical measurement data in the shape of $(L/K) \times N$ into low-resolution electrical images of a 2-dimensional N-channel are similar to the steps for converting high resolution electrical images. Specifically, by replacing the high frequencies and high resolutions mentioned in the high-resolution electrical image conversion process with low frequencies and low resolutions, and replacing l in step 3 of Table 2 with $(l/\sqrt{K})$, low resolution electrical images of M 2-dimensional N-channel can be obtained. Each channel is a 2-dimensional matrix with rows multiplied by columns $(l/\sqrt{K}) \times (l/\sqrt{K})$.

In this study, the sampling frequencies of low-frequency and high-frequency electrical measurement data are 15 min and 1 min, respectively. To facilitate the calculation process in constructing electrical images, a value of 0 is added every 15 data points so that the reconstruction factor K changes from 15 to 16 and $\sqrt{K}$ is an integer. Such adding zero operation will not affect the conversion of low-resolution electrical images. Consequently, the electrical measurement data is converted into one electrical image every 64 hours, wherein the length and width of each channel of the high-resolution electrical image is $l = 64$, and the length and width of each channel of the low-resolution electrical image is $l/\sqrt{K} = 16$. All the mentioned datasets are transformed into 180 high-resolution electrical images and 180 low-resolution electrical images. The training set and test set are divided in an 8: 1 ratio.

B. EVALUATION INDEX

Electrical images are highly structured, meaning that there is a strong correlation between adjacent pixels. This paper takes structural similarity (SSIM) [34] as the index for evaluating the reconstruction accuracy of electrical images from the perspective of image structure, in which the mean value is used as the estimation of brightness, the standard deviation as the estimation of contrast, and the covariance as the measurement of structural similarity. Thus, SSIM can offset the defects of

MSE in measuring the similarity of image structure, as

$$SSIM(x_m^{\mathrm{HR}}, x_m^{\mathrm{SR}}) = \frac{2\mu_{x_m^{\mathrm{HR}}}\mu_{x_m^{\mathrm{SR}}} + C_1}{\mu_{x_m^{\mathrm{HR}}}^2 + \mu_{x_m^{\mathrm{SR}}}^2 + C_1} \times \frac{2\sigma_{x_m^{\mathrm{HR}}x_m^{\mathrm{SR}}} + C_2}{\sigma_{x_m^{\mathrm{HR}}}^2 + \sigma_{x_m^{\mathrm{SR}}}^2 + C_2} \quad (9)$$

where $\mu_{x_m^{\mathrm{HR}}}$ and $\mu_{x_m^{\mathrm{SR}}}$ are the average values of x_m^{HR} and x_m^{SR} respectively while $\sigma_{x_m^{\mathrm{HR}}}$ and $\sigma_{x_m^{\mathrm{SR}}}$ are the standard deviations of x_m^{HR} and x_m^{SR}, respectively. $\sigma_{x_m^{\mathrm{HR}}x_m^{\mathrm{SR}}}$ is the covariance of x_m^{HR} and x_m^{SR}. C_1 and C_2 are constants, where $C_1 = (0.01 \times 255)^2$, and $C_2 = (0.03 \times 255)^2$. It can be seen that the value range of SSIM is [0, 1] while the larger the SSIM is, the more closely-correlated the internal structures between the super-resolution and the high-resolution electrical image will be regarding the texture and hue, implying the corresponding similarity in changing trend and numerical size of the electrical measurement data, respectively.

Besides, peak signal-to-noise ratio (PSNR) [35] is taken as indicator for evaluating reconstruction quality in image compression and image reconstruction. PSNR is defined by MSE. The higher the PSNR, the smaller the MSE, and the smaller the distortion from the perspective of power image or electrical measurement data, which can be calculated as

$$PSNR(x_m^{\mathrm{HR}}, x_m^{\mathrm{SR}}) = 10\log_{10}\frac{255^2}{MSE(x_m^{\mathrm{HR}}, x_m^{\mathrm{SR}})} \quad (10)$$

$$MSE(x_m^{\mathrm{HR}}, x_m^{\mathrm{SR}}) = \frac{1}{l^2}\sum_{w=1}^{l}\sum_{h=1}^{l}((x_m^{\mathrm{HR}})_{w,h} - (x_m^{\mathrm{SR}})_{w,h})^2 \quad (11)$$

C. COMPARISON BETWEEN SUPER-RESOLUTION RECONSTRUCTION AND INTERPOLATION RECONSTRUCTION

Comparisons between the super-resolution reconstruction and the bicubic interpolation (BI) [36] reconstruction are conducted from the following five aspects.

1) VISUAL ASSESSMENT

Figure 8 shows the results of super-resolution reconstruction and interpolation reconstruction. In this study, the four building datasets are individually trained and tested. Figures 8 (a)-(d) show the last electrical image of the test set. In terms of the amount of electrical data, high-resolution electrical images are 16 times that of low-resolution electrical images. The high-resolution electrical image has 64 electrical data per line, while the low-resolution electrical image has only 16 electrical data per line, resulting in the low-resolution electrical image being visually blurred. In addition to the overall color distribution of low-resolution electrical images, high-resolution electrical images are also visually rich in high-frequency details and clear textures. Although the pixels of the interpolation-reconstructed electrical image have

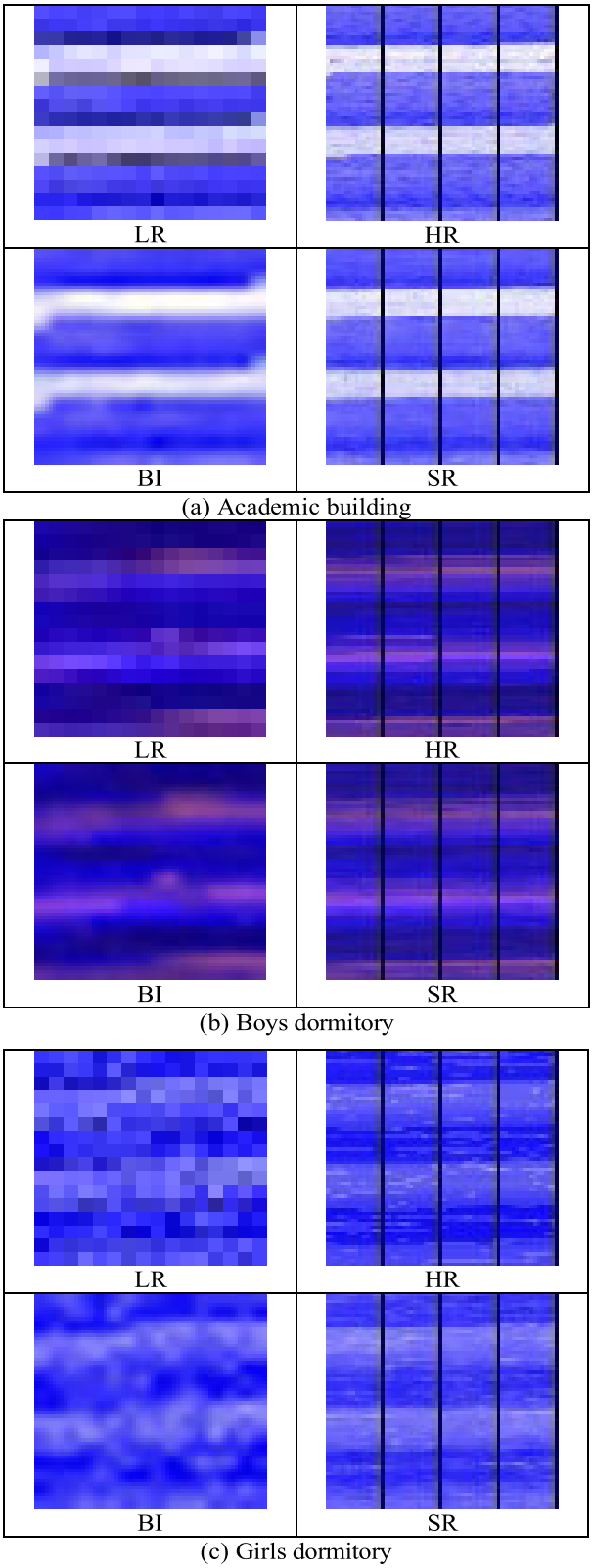

FIGURE 8. Results of super resolution reconstruction and interpolation reconstruction (electrical image). Acronyms: LR→Low resolution electrical image, HR→High resolution electrical image, BI→Electrical image reconstructed by bicubic interpolation, SR→Super resolution electrical image.

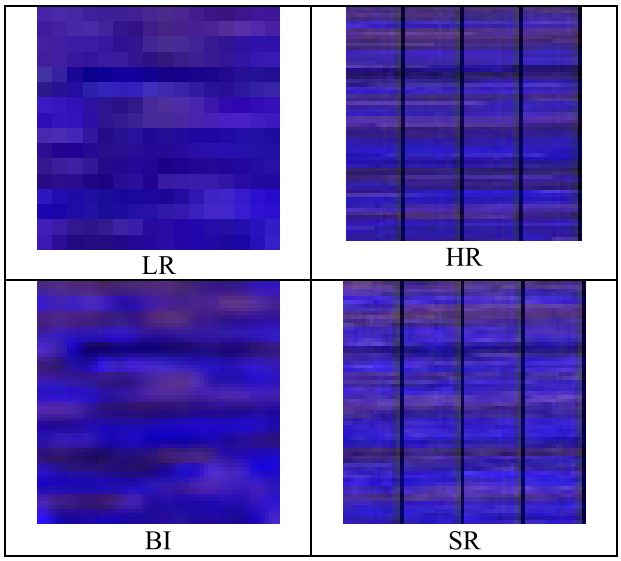

(d) Restaurant

FIGURE 8. *(Continued.)* **Results of super resolution reconstruction and interpolation reconstruction (electrical image). Acronyms: LR→Low resolution electrical image, HR→High resolution electrical image, BI→Electrical image reconstructed by bicubic interpolation, SR→Super resolution electrical image.**

increased, they are smooth visually, and the reconstruction effect is relatively conservative, indicating that the interpolation reconstruction method does not have the ability to restore high-frequency details. By contrast, the texture of the super-resolution electrical image has a very high similarity with the texture of the high-resolution electrical image, indicating that the high-frequency details of the super-resolution reconstruction have a high reconstruction quality. It can be seen that the super-resolution reconstruction method can achieve a good reconstruction effect for the electrical measurement data from different buildings in the same geographical location.

2) OBJECTIVE ASSESSMENT

Calculate the PSNR and SSIM of real samples and generated samples by formulas (8)-(10), and take the average value as the final evaluation index, as shown in Table 4. Note that for the electrical measurement data sets of different buildings, the PSNR of super-resolution reconstruction is relatively high, indicating that the reconstruction result of this method is less distorted. The SSIMs involved in super-resolution reconstruction are around 0.9, indicating that the method can learn the structural relationship of electrical images including texture and hue, thereby effectively recovering high-frequency details of electrical measurement data. However, the values of PSNR and SSIM of the interpolated reconstruction are relatively small, indicating that the method cannot effectively extract the data structure relationship of the electrical image so that the restoration of high-frequency details for the electrical measurement data is insufficient.

TABLE 4. Evaluation of reconstruction accuracy for different reconstruction methods.

Reconstruction method	Evaluation index	Test set			
		Acad	Boys	Girls	Rest
SR	PSNR	**25.85**	**29.42**	**24.72**	**27.11**
	SSIM	**0.97**	**0.95**	**0.91**	**0.89**
BI	PSNR	13.72	17.51	15.45	17.41
	SSIM	0.48	0.57	0.42	0.40

Acronyms: Acad→Academic building, Boys→Boys dormitory, Girls→Girls dormitory, Rest→Restaurant.

3) TREND OF TIME SERIES DATA

The electrical image of the test set is flattened into electrical measurement data in the form of time series, as shown in Figure 9. The comparison between the reconstructed curve and the real curve shows that, except for the high peaks or low valleys in individual intervals, the trends of the two curves are basically the same, indicating that the proposed method can recover the edge details of the low frequency electrical measurement data.

4) STATISTICAL CHARACTERISTICS

In this article, two important characteristics of reconstructed data are discussed.

(i) Distribution similarity. This study verifies that the reconstructed data has the same statistical characteristics as the real data. In Figure 10, with the academic building as the research object, this section shows the cumulative distribution function (CDF) of real data and reconstructed data. It can be seen that the CDF of the real data and the reconstructed data almost overlap. It can be concluded that the super-resolution reconstruction method can reconstruct data with correct marginal distribution.

(ii) Spatial correlation: In order to further verify the reconstruction quality, this section calculates the spatial correlation coefficient of academic building, boys dormitory, girls dormitory and restaurant at the same time, as shown in Figure 11. It can be seen that even if the reconstruction models of each building are trained separately, the spatial correlation of the reconstructed data is consistent with the real data.

5) NOISE ROBUSTNESS

In practical applications, the data has a slight deviation after being polluted by noise during the communication process. In this article, the duration of each electrical image is 64 hours. In order to verify the noise robustness of the proposed method, it is set that the communication instability occurs for 1 hour every 24 hours and causes a noise deviation of 10%, 20%, and 30%. In addition, consider a more serious situation, which is that communication instability continues throughout the whole period and causes 10%, 20%, and 30% noise deviation. Take the academic building data set for simulation.

The evaluation of reconstruction accuracy considering noise pollution is shown in Table 5. It can be seen that in the case of a 10%, 20%, 30% noise deviation every 24 hours

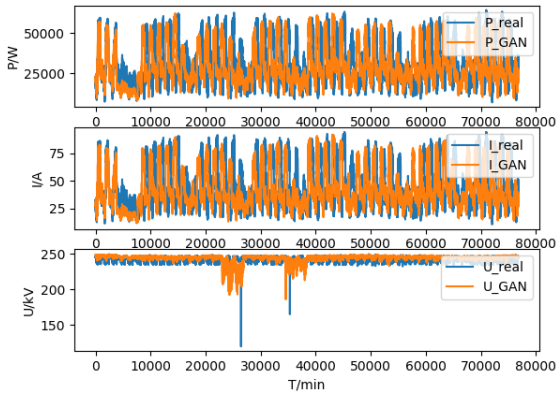

(a) Academic building

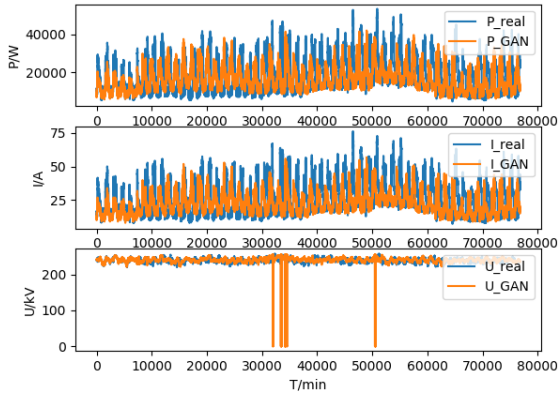

(b) Boys dormitory

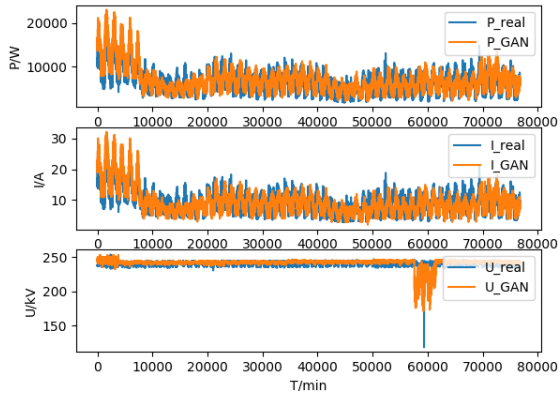

(c) Girls dormitory

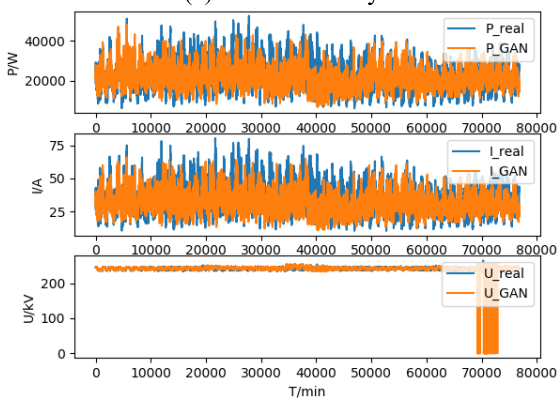

(d) Restaurant

FIGURE 9. Results of super resolution reconstruction (time series).

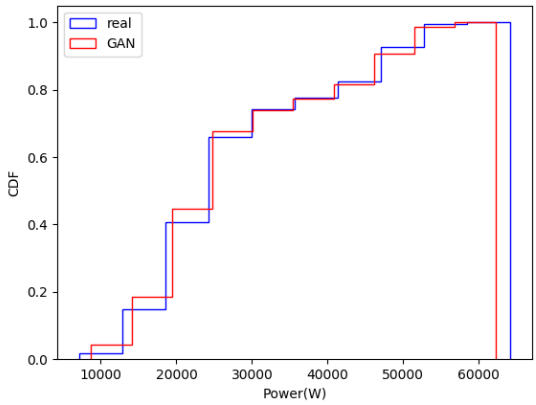

(a) Active power

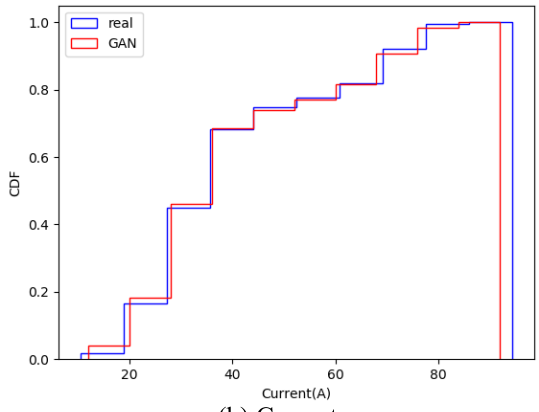

(b) Current

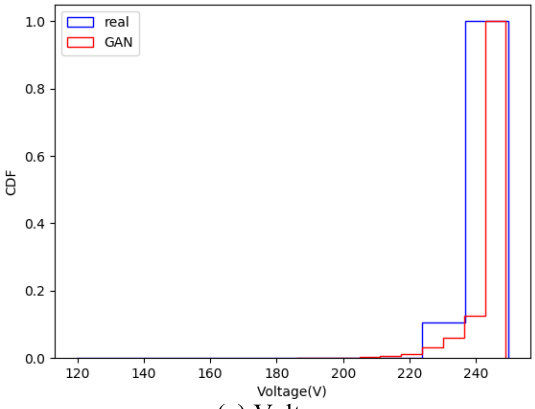

(c) Voltage

FIGURE 10. Results of CDF.

for 1 hour, the proposed method can obtain high quality and good stability evaluation results. It shows that the proposed method can effectively overcome the local noise in the data communication process and has strong local noise robustness. In addition, in the case of continuous 10%, 20%, and 30% noise deviations throughout the period, although the reconstruction accuracy of the proposed method shows a downward trend, it still has higher PSNR and SSIM in the case of 10% and 20% noise. It shows that the proposed method also has strong noise robustness in the whole period.

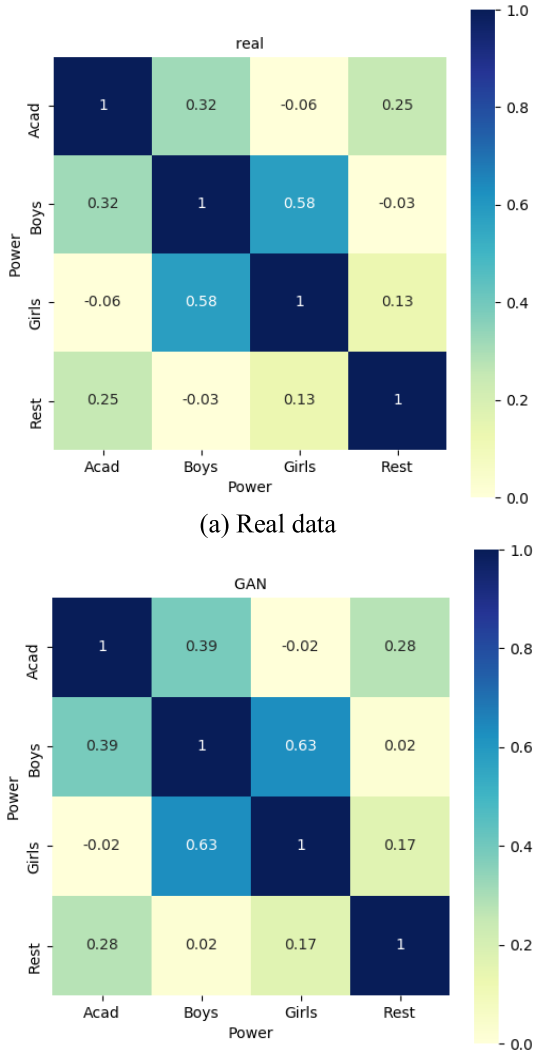

(a) Real data

(b) Reconstruction data

FIGURE 11. Heat map of the spatial correlation coefficient.

TABLE 5. Evaluation of reconstruction accuracy considering noise pollution.

Evaluation index	Noise in local periods			Noise in the whole period		
	10%	20%	30%	10%	20%	30%
PSNR	25.73	25.64	25.57	25.28	24.30	22.95
SSIM	0.97	0.97	0.96	0.97	0.96	0.95

D. THE GENERALIZATION OF THE MODEL IN THIS PAPER BETWEEN DIFFERENT DATA SETS IN THE SAME REGION

In this section, the electrical measurement data of different buildings in the same geographic location are trained separately. After that, study the generalization of the trained model to the electrical measurement data of other buildings. Specifically, this case uses datasets from four buildings in the same school, including academic building, boys dormitory, girls dormitory, and restaurant. To the best of our knowledge, the previous case has trained the reconstruction

TABLE 6. Evaluation of reconstruction accuracy for different datasets at the same location.

Trained model	Evaluation index	Test set			
		Acad	Boys	Girls	Rest
Acad	PSNR	**25.85**	13.61	**23.01**	14.10
	SSIM	**0.97**	0.58	**0.89**	0.58
Boys	PSNR	14.21	**29.42**	19.67	**27.13**
	SSIM	0.72	**0.95**	0.75	**0.89**
Girls	PSNR	**24.81**	18.94	**24.72**	19.09
	SSIM	**0.96**	0.73	**0.91**	0.70
Rest	PSNR	12.25	**26.91**	18.58	**27.11**
	SSIM	0.60	**0.92**	0.72	**0.89**

Acronyms: Acad→Academic building, Boys→Boys dormitory, Girls→Girls dormitory, Rest→Restaurant.

models for the datasets of the four buildings. In order to study the generalization of the reconstruction model between different datasets in the same region, this section cross-inputs the test sets of four buildings into the four reconstruction models. The generalization ability testing results are shown in Figure 12. It can be seen that the reconstruction model of academic building has a good performance (i.e., a good generalization ability) when datasets for girls' dormitory are used as the testbed but poor results for boys' dormitory and dinning datasets. Similar observations can also be obtained when we look into the generalization ability of girls' dormitory reconstruction model to academic building's datasets, boys' dormitory model to dinning's datasets and dinning's model to boys' dormitory datasets. This demonstrates that electricity consumption behaviors in academic building and girls dormitory are similar and closely-correlated, as well as those in the boys dormitory and restaurant.

To understand the deeper reason, PSNR and SSIM is the above generalization ability test are calculated as shown in Table 6. It can be seen that the test datasets of girls' dormitory have higher PSNR and SSIM on the academic building's reconstruction model than on the others, while the same conclusions can also be drawn from the test of academic building's data on girls' model and the mutual test of boys' dormitory and restaurant models/datasets. This again implies a similar data structures and justifies the super-resolution reconstruction method can generalize between different data sets with similar structural relationships in the same region.

E. VERSATILITY OF RECONSTRUCTION MODELS FOR DATA SETS IN DIFFERENT REGIONS

At the beginning of this section, we separately train super-resolution reconstruction models with datasets from different geographic locations. Immediately afterwards, the test sets of different geographic locations are input into each trained reconstruction model. In the end, according to the reconstruction results, we evaluate the versatility and generalization of the proposed method in different geographic locations. In Table 7, the model trained with AMPds2 has higher PSNR and SSIM on the AMPds2 test set. Similarly, models trained with IHEPCds have higher PSNR and SSIM on the IHEPCds test set. However, when used to test other

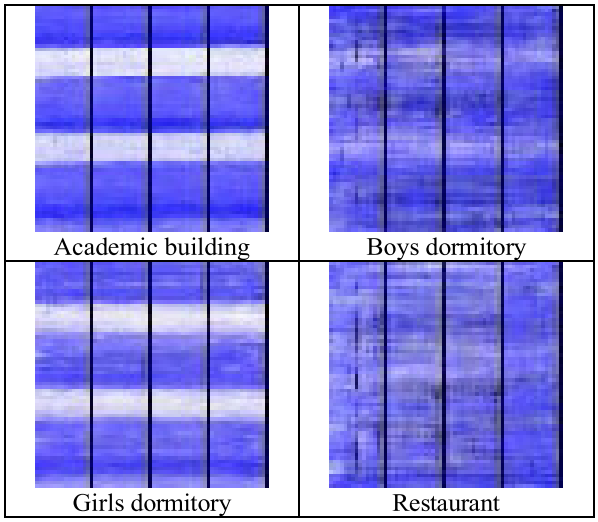

(a)Test set of Academic building

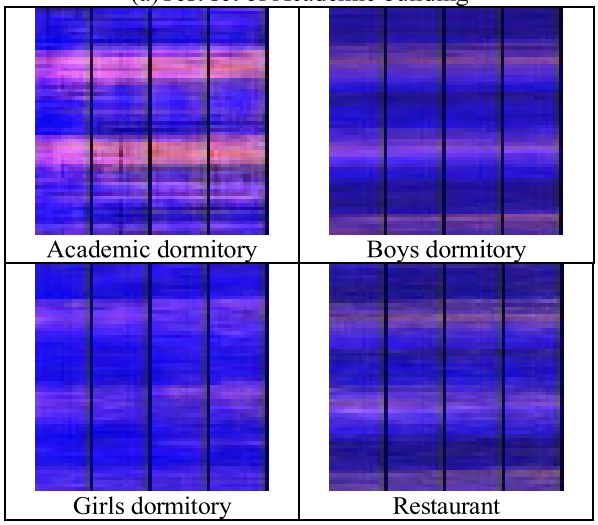

(b) Test set of Boys dormitory

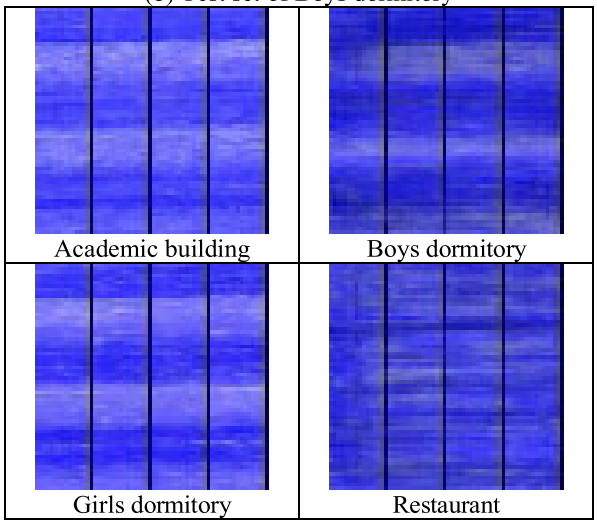

(c) Test set of Girls dormitory

FIGURE 12. Results of super resolution reconstruction for different datasets at the same location (electrical image).

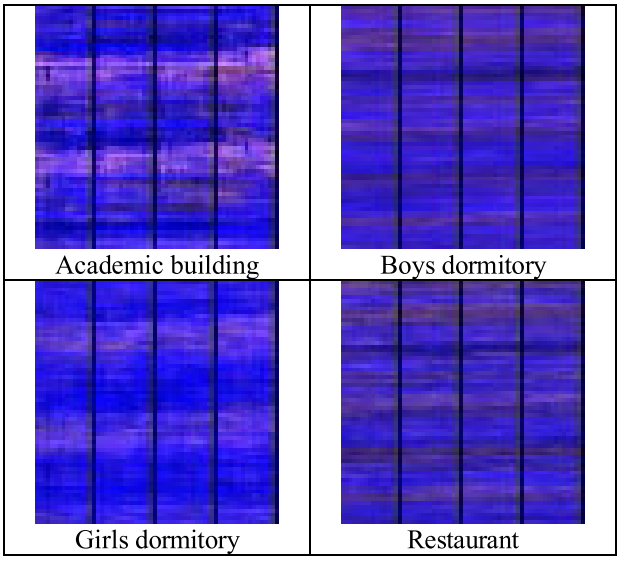

(d) Test set of Restaurant

FIGURE 12. *(Continued.)* Results of super resolution reconstruction for different datasets at the same location (electrical image).

TABLE 7. Evaluation of reconstruction accuracy for datasets at different locations.

Trained model	Evaluation index	Test set		
		I-BLEND	AMPds2	IHEPCds
I-BLEND	PSNR	**27.11**	14.14	15.47
	SSIM	**0.89**	0.49	0.58
AMPds2	PSNR	11.18	**23.76**	0.79
	SSIM	0.40	**0.72**	0.23
IHEPCds	PSNR	15.76	14.77	**21.66**
	SSIM	0.60	0.15	**0.70**

geographic datasets, the PSNR and SSIM of the trained I-BLEND, AMPds2, or IHEPCds models are relatively low. The results show AAthat the proposed method is applicable to the reconstruction of datasets in different geographic locations and can achieve satisfactory reconstruction results. However, the proposed method lacks generalization between datasets in different geographic locations. It is speculated that the user and electricity consumption behaviors of datasets in different geographic locations have obvious differences, resulting in no similar potential distribution between data sets in different geographic locations. To our knowledge, it is contrary to the fact that GAN essentially reconstructs data by mining the potential distribution of data [18].

V. CONCLUSION

In this paper, a generative adversarial network based super-resolution reconstruction method for low-frequency electrical measurement data of smart grid is proposed. The main advantages are as follows.

1) A method for transforming electrical measurement data into electrical images is designed so that the GAN can effectively learn the potential distribution of electrical measurement data with the help of image processing techniques.

It realizes the effective combination of electrical field and image field.

2) The Wasserstein distance is introduced into the GAN model to avoid the disappearance of the gradient of the GAN, which improves the training stability.

3) Three designs are involved, including a generator based on deep residual network, a discriminator based on deep convolutional network, and a perceptual loss function, and simulation shows that they result in high reconstruction accuracy and restore rich high-frequency detail.

4) The proposed method is a data-driven based unsupervised training method with no need to model the electrical measurement data. The trained reconstruction model can be generalized to different datasets in the same geographical location. In addition, the proposed method is also universal for datasets from different geographical locations.

In order to further enhance the generalization ability between different geographic datasets, we will consider to establish a broad and common knowledge map by mining the knowledge representation of electrical data in different regions, and realize the key knowledge interaction among data in different regions through transfer learning.

REFERENCES

[1] X. Fang, S. Misra, G. Xue, and D. Yang, "Smart grid—The new and improved power grid: A survey," *IEEE Commun. Surveys Tuts.*, vol. 14, no. 4, pp. 944–980, Qua. 2012.

[2] V. C. Gungor, D. Sahin, T. Kocak, S. Ergut, C. Buccella, C. Cecati, and G. P. Hancke, "Smart grid technologies: Communication technologies and standards," *IEEE Trans. Ind. Informat.*, vol. 7, no. 4, pp. 529–539, Nov. 2011.

[3] K. Zhou, C. Fu, and S. Yang, "Big data driven smart energy management: From big data to big insights," *Renew. Sustain. Energy Rev.*, vol. 56, pp. 215–225, Apr. 2016.

[4] D. Xu, Q. Wu, B. Zhou, C. Li, L. Bai, and S. Huang, "Distributed multi-energy operation of coupled electricity, heating and natural gas networks," *IEEE Trans. Sustain. Energy*, early access, Dec. 23, 2019, doi: 10.1109/TSTE.2019.2961432.

[5] D. Xu, B. Zhou, Q. Wu, C. Y. Chung, C. Li, S. Huang, and S. Chen, "Integrated modelling and enhanced utilization of Power-to-Ammonia for high renewable penetrated multi-energy systems," *IEEE Trans. Power Syst.*, early access, Apr. 22, 2020, doi: 10.1109/TPWRS.2020.2989533.

[6] L. Xi, T. Yu, B. Yang, X. Zhang, and X. Qiu, "A wolf pack hunting strategy based virtual tribes control for automatic generation control of smart grid," *Appl. Energy*, vol. 178, pp. 198–211, Sep. 2016.

[7] L. Das, D. Garg, and B. Srinivasan, "NeuralCompression: A machine learning approach to compress high frequency measurements in smart grid," *Appl. Energy*, vol. 257, Jan. 2020, Art. no. 113966.

[8] S. M. S. Alam, B. Natarajan, and A. Pahwa, "Distribution grid state estimation from compressed measurements," *IEEE Trans. Smart Grid*, vol. 5, no. 4, pp. 1631–1642, Jul. 2014.

[9] F. Zhang, L. Cheng, X. Li, Y. Sun, W. Gao, and W. Zhao, "Application of a real-time data compression and adapted protocol technique for WAMS," *IEEE Trans. Power Syst.*, vol. 30, no. 2, pp. 653–662, Mar. 2015.

[10] V. Miranda, J. Krstulovic, H. Keko, C. Moreira, and J. Pereira, "Reconstructing missing data in state estimation with autoencoders," *IEEE Trans. Power Syst.*, vol. 27, no. 2, pp. 604–611, May 2012.

[11] S. Wang, H. Chen, and Z. Pan, "A reconstruction method for missing data in power system measurement using an improved generative adversarial network," *Proc. CSEE*, vol. 39, no. 1, pp. 56–64, 2019.

[12] T. Yang, Y. Li, and Z. He, "Matrix completion theory based recovery algorithm for power quality data in ubiquitous power Internet of Things," *Automat. Electr. Power Syst.*, vol. 44, no. 2, pp. 13–22, 2020.

[13] S. Liang, W. Fang, and J. Wang, "Refinement and anomaly detection for power consumption data based on recovery of graph regularized low-rank Matrix," *Autom. Electr. Power Syst.*, vol. 43, no. 21, pp. 221–228, 2019.

[14] L. Wang, S. Xiang, G. Meng, H. Wu, and C. Pan, "Edge-directed single-image super-resolution via adaptive gradient magnitude self-interpolation," *IEEE Trans. Circuits Syst. Video Technol.*, vol. 23, no. 8, pp. 1289–1299, Aug. 2013.

[15] S. D. Babacan, R. Molina, and A. K. Katsaggelos, "Variational Bayesian super resolution," *IEEE Trans. Image Process.*, vol. 20, no. 4, pp. 984–999, Apr. 2011.

[16] T. Lukeš, P. Křížek, Z. Švindrych, J. Benda, M. Ovesný, K. Fliegel, M. Klíma, and G. M. Hagen, "Three-dimensional super-resolution structured illumination microscopy with maximum a posteriori probability image estimation," *Opt. Express*, vol. 22, no. 24, p. 29805, Dec. 2014.

[17] X. Lu, Y. Yuan, and P. Yan, "Alternatively constrained dictionary learning for image super resolution," *IEEE Trans. Cybern.*, vol. 44, no. 3, pp. 366–377, Mar. 2014.

[18] I. J. Goodfellow, J. Pouget-Abadie, M. Mirza, B. Xu, D. Warde-Farley, S. Ozair, A. Courville, and Y. Bengio, "Generative adversarial networks," in *Proc. Adv. Neural Inf. Process. Syst.*, vol. 3, 2014, pp. 2672–2680.

[19] K. Bousmalis, N. Silberman, D. Dohan, D. Erhan, and D. Krishnan, "Unsupervised pixel-level domain adaptation with generative adversarial networks," in *Proc. IEEE Conf. Comput. Vis. Pattern Recognit. (CVPR)*, Jul. 2017, pp. 3722–3731.

[20] H. Zhang, T. Xu, H. Li, S. Zhang, X. Wang, X. Huang, and D. Metaxas, "StackGAN: Text to photo-realistic image synthesis with stacked generative adversarial networks," in *Proc. IEEE Int. Conf. Comput. Vis. (ICCV)*, Venice, Italy, Oct. 2017, pp. 5907–5915.

[21] Y. Chen, Y. Wang, D. Kirschen, and B. Zhang, "Model-free renewable scenario generation using generative adversarial networks," *IEEE Trans. Power Syst.*, vol. 33, no. 3, pp. 3265–3275, May 2018.

[22] F. Zhou, S. Yang, H. Fujita, D. Chen, and C. Wen, "Deep learning fault diagnosis method based on global optimization GAN for unbalanced data," *Knowl.-Based Syst.*, vol. 187, Jan. 2020, Art. no. 104837.

[23] M. Arjovsky, S. Chintala, and L. Bottou, "Wasserstein GAN," 2017, *arXiv:1701.07875*. [Online]. Available: https://arxiv.org/abs/1701.07875

[24] C. Ledig, L. Theis, F. Huszar, J. Caballero, A. Cunningham, A. Acosta, A. Aitken, A. Tejani, J. Totz, Z. Wang, and W. Shi, "Photo-realistic single image super-resolution using a generative adversarial network," in *Proc. IEEE Conf. Comput. Vis. Pattern Recognit. (CVPR)*, Venice, Italy, Jul. 2017, pp. 4681–4690.

[25] A. S. N. Uttama Nambi, A. Reyes Lua, and V. R. Prasad, "LocED: Location-aware energy disaggregation framework," in *Proc. 2nd ACM Int. Conf. Embedded Syst. Energy-Efficient Built Environments BuildSys*, 2015, pp. 45–54.

[26] G. Hebrail and A. Barard. (2006). *Individual Household Electric Power Consumption Dat Set(IHEPCds)*. [Online]. Available: https://archive.ics.uci.edu/ml/datasets/Individual+household+electric+power+consumption

[27] S. Makonin, F. Popowich, L. Bartram, B. Gill, and I. V. Bajic, "AMPds: A public dataset for load disaggregation and eco-feedback research," in *Proc. IEEE Electr. Power Energy Conf.*, Aug. 2013, pp. 1–6.

[28] H. Rashid, P. Singh, and A. Singh, "I-BLEND, a campus-scale commercial and residential buildings electrical energy dataset," *Sci. Data*, vol. 6, no. 1, Mar. 2019, Art. no. 190015.

[29] DECC, UK Government. (2012). *Smart Metering Equipment Technical Specifications: Version 2*. [Online]. Available: http://bit.ly/1401o61

[30] K. Wang, C. Gou, Y. Duan, Y. Lin, X. Zheng, and F.-Y. Wang, "Generative adversarial networks: The state of the art and beyond," (in Chinese), *Acta Autom. Sinica*, vol. 43, no. 2, pp. 321–332, 2017.

[31] K. He, X. Zhang, S. Ren, and J. Sun, "Deep residual learning for image recognition," in *Proc. IEEE Conf. Comput. Vis. Pattern Recognit. (CVPR)*, Las Vegas, NV, USA, Jun. 2016, pp. 770–778.

[32] K. Simonyan and A. Zisserman, "Very deep convolutional networks for large-scale image recognition," 2014, *arXiv:1409.1556*. [Online]. Available: https://arxiv.org/abs/1409.1556

[33] A. Krizhevsky, I. Sutskever, and G. Hinton, "ImageNet classification with deep convolutional neural networks," in *Proc. Adv. Neural Inf. Process. Syst. (NIPS)*, Lake Tahoe, America, 2012. pp. 1097–1105.

[34] Z. Wang, A. C. Bovik, H. R. Sheikh, and E. P. Simoncelli, "Image quality assessment: From error visibility to structural similarity," *IEEE Trans. Image Process.*, vol. 13, no. 4, pp. 600–612, Apr. 2004.

[35] S. Welstead, "Fractal and wavelet image compression techniques," in *Storage & Retrieval for Image & Video Databases*. Newport Beach, CA, USA: Society of Photo-Optical Instrumentation Engineers, 1999.

[36] R. E. Carlson and F. N. Fritsch, "Monotone piecewise bicubic interpolation," *SIAM J. Numer. Anal.*, vol. 22, no. 2, pp. 386–400, Apr. 1985.

FUSHENG LI received the B.Eng. degree in electrical engineering from the South China University of Technology, Guangzhou, China, in 2018, where he is currently pursuing the M.S. degree with the School of Electric Power Engineering. His research interests include artificial intelligence techniques and its application in smart grid.

DAN LIN received the B.Eng. degree in electrical engineering from the South China University of Technology, Guangzhou, China, in 2018, where she is currently pursuing the M.S. degree with the School of Electric Power Engineering. Her research interests include distribution planning and reliability assessment, and artificial intelligence techniques.

TAO YU (Member, IEEE) received the B.Eng. degree in electrical power system from Zhejiang University, Hangzhou, China, in 1996, the M.Eng. degree in hydroelectric engineering from Yunnan Polytechnic University, Kunming, China, in 1999, and the Ph.D. degree in electrical engineering from Tsinghua University, Beijing, China, in 2003. He is currently a Professor with the College of Electric Power, South China University of Technology, Guangzhou, China. His research interests include nonlinear and coordinated control theory, artificial intelligence techniques, and operation of power systems.